Published in final edited form as:

Adv Healthc Mater. 2016 March ; 5(6): 676–687. doi:10.1002/adhm.201500758.

Integration of 3D Printed and Micropatterned Polycaprolactone Scaffolds for Guidance of Oriented Collagenous Tissue Formation *In vivo*

Sophia P Pilipchuk,
Department of Biomedical Engineering, 1101 Beal Ave., University of Michigan, Ann Arbor, MI 48109, USA

Department of Periodontics and Oral Medicine, 1011 N. University Ave., University of Michigan, Ann Arbor, MI 48109, USA

Alberto Monje,
Department of Periodontics and Oral Medicine, 1011 N. University Ave., University of Michigan, Ann Arbor, MI 48109, USA

Yizu Jiao,
Department of Periodontics and Oral Medicine, 1011 N. University Ave., University of Michigan, Ann Arbor, MI 48109, USA

Jie Hao,
Department of Periodontics and Oral Medicine, 1011 N. University Ave., University of Michigan, Ann Arbor, MI 48109, USA

Laura Kruger,
Department of Periodontics and Oral Medicine, 1011 N. University Ave., University of Michigan, Ann Arbor, MI 48109, USA

Colleen L Flanagan,
Department of Biomedical Engineering, 1101 Beal Ave., University of Michigan, Ann Arbor, MI 48109, USA

Scott J Hollister, and
Department of Biomedical Engineering, 1101 Beal Ave., University of Michigan, Ann Arbor, MI 48109, USA

Department of Mechanical Engineering, Department of Surgery, University of Michigan, Ann Arbor, MI 48109, USA

William V Giannobile
Department of Biomedical Engineering, 1101 Beal Ave., University of Michigan, Ann Arbor, MI 48109, USA

Correspondence to: William V Giannobile, wgiannob@umich.edu.

Supporting Information

Supporting Information is available from the Wiley Online Library or from the author.

Department of Periodontics and Oral Medicine, 1011 N. University Ave., University of Michigan, Ann Arbor, MI 48109, USA

William V Giannobile: wgiannob@umich.edu

Abstract

Scaffold design incorporating multi-scale cues for clinically-relevant, aligned tissue regeneration has potential to improve structural and functional integrity of multi-tissue interfaces. The objective of this pre-clinical study was to develop poly(ε-caprolactone) (PCL) scaffolds with mesoscale and microscale architectural cues specific to human ligament progenitor cells and assess their ability to form aligned bone-ligament-cementum complexes *in vivo*. PCL scaffolds were designed to integrate a 3D printed bone region with a micropatterned PCL thin film consisting of grooved pillars. The patterned film region was seeded with human ligament cells, fibroblasts transduced with BMP-7 genes seeded within the bone region, and a tooth dentin segment positioned on the ligament region prior to subcutaneous implantation into a murine model. Results indicated increased tissue alignment *in vivo* using micropatterned PCL films, compared to random-porous PCL. At 6 weeks, 30um groove depth significantly enhanced oriented collagen fiber thickness, overall cell alignment, and nuclear elongation relative to 10um groove depth. This study demonstrates for the first time that scaffolds with combined hierarchical mesoscale and microscale features can align cells *in vivo* for oral tissue repair with potential for improving the regenerative response of other bone-ligament complexes.

Keywords

micropatterning; polycaprolactone (PCL); periodontal ligament (PDL); cell alignment; 3D printing

1. Introduction

Formation of tissues with structural and functional integrity is reliant upon cellular alignment and organization that in turn is influenced by nano- and micro-scale environmental cues.[1] Soft collagenous tissues such as tendon and ligament require aligned collagen fiber formation to maintain resistance to mechanical loading. Similarly, the periodontal ligament (PDL) is a structure in the oral cavity composed primarily of collagen type III which anchors alveolar bone to the tooth root and resists compressive loading--allowing for tooth movement. Periodontitis is a chronic oral inflammatory disease associated with damage to the tooth-supporting apparatus and subsequent osseous tissue resorption. It is the primary cause of permanent tooth loss estimated to affect 47.2% of adults in the United States, with a prevalence of 70% for adults aged 65 years and older.[2] Tissue engineering strategies have shown potential to address existing deficiencies in clinically-induced periodontal regeneration through combinational approaches using biomaterials, growth factors, and cell-based therapy.[3] Existing studies have focused on whether precise topographical mesoscale features can influence structural and functional properties of PDL-like tissue through contact guidance *in vitro*.[4, 5] However, their further translation and performance *in vivo* has not yet been described, yet is needed to optimize scaffold constructs for oriented, multi-tissue interface regeneration.

The complex hierarchical organization of periodontal tissues requires multi-phasic biomaterial constructs that can recapitulate the structural integrity of the bone-ligament interface.[6] Microscale technologies have been used in fabricating scaffolds that facilitate control of multiple tissue organization and positioning, as required for the regeneration of a bone-ligament interface.[7] Surface topography on the micro- and nano-scale profoundly affects cell behavior, including adhesion, migration, alignment, intracellular signaling pathways, and ultimately tissue formation in combination with biochemical cues. As such, there is a growing emphasis being placed on a multiscale approach to scaffold development that should incorporate strategically-positioned, biologically-relevant design features ranging from the nano- to the macro-scale.[8] Fabricating scaffolds sufficient for clinical application remains a challenge for tissue engineering of multi-phase, oriented tissue interfaces.

Polycaprolactone (PCL)—a hydrolytically-biodegradable polyester approved by the FDA for some clinical indications—is easily manufactured into a variety of shapes and porosities with variable mechanical properties and has been the material of choice in multi-phasic scaffolds for regeneration of periodontia. Park et al. used 3-D printed wax-based molds to cast PCL for a “bone compartment” of an image-based, bi-phasic scaffold “periodontal complex”.[9, 10] Costa et al. and Vaquette et al. employed PCL for the bone compartment and electrospun PCL for the PDL region,[11] while Lee et al. used a layered 3-D printed scaffold with three PCL interphases for the cementum, PDL, and alveolar bone.[12] However, the precise effect of topography on the guidance of PDL-like tissue formation *in vivo* has not been thoroughly explored to understand how micro-scale patterning affects the regenerative outcome.

The objective of this study was to develop a scaffold with micro- and macro-scale cues for guided formation of aligned tissue that would meet design criteria for periodontal ligament-like architecture. Given PCL's malleability and ability to be formed into polymeric matrices of various physical and mechanical properties, 2D PCL films were micropatterned and assessed *in vitro* to determine optimal parameters for PDL cell alignment. This informed the design of a 3D PCL film having 250um high pillars to replicate the average thickness of PDL tissue, with grooves embedded into the pillars at widths of 15–60um and depths of 10–30um. Films were incorporated into a 3D printed PCL region to create a macro-scale bone-ligament interphase reminiscent of the alveolar bone-PDL complex in the oral cavity. We integrated 3D printed and micropatterned regions to develop a multi-tissue interphase with macro- and micro-specific features of the scaffold. We then examined the potential of the designed scaffold construct for guidance of mineralized (bone, cementum) and collagenous (PDL-like) tissue formation using subcutaneous implantation in an ex vivo model. Our findings identify the importance of grooved features and the influence of their depths on cellular alignment, elongation, and oriented collagenous tissue formation *in vivo*.

2. Results

2.1 PCL surface treatment and ligament cell alignment on 2D grooved PCL films

Four different surface treatments of non-patterned PCL films were performed prior to cell seeding to assess periodontal ligament (PDL) cell adhesion and proliferation relative to non-

treated films: (1) amination to generate a PCL-NH_2 surface chemistry, (2) hydrolysis to reduce surface hydrophobicity, (3) fibronectin, and (4) hydrolysis pre-treatment prior to fibronectin coating. Significantly higher mean hPDL cell adhesion percentage of the initial cell seeding density was shown using treatment of PCL with fibronectin alone and a combined treatment of hydrolysis and fibronectin at day 1 post-seeding, relative to a non-treated PCL film. At day 5, the total percentage of adhered cells was significantly higher on hydrolysis, fibronectin, and combined hydrolysis and fibronectin treatment of PCL surfaces relative to amination and no treatment (Figure 1). Based on these results, all PCL patterned and control films were hydrolyzed the day before and fibronectin-coated the day of hPDL cell seeding to increase cell attachment to the inert PCL surface.

To create a 3D micropattern design for the PDL region of the scaffold, a 2D pattern was first generated to study the parameters that assisted in periodontal progenitor cell alignment. Three different molds were fabricated using three groove widths ranging from 10–50um, with a depth of 10um (Figure 2A). PCL was readily patterned, replicating mold features and creating a film that can be easily handled without distorting the features (Figure 2B). Human PDL cells seeded onto the surface treated, patterned films showed elongation of filopodia within the grooves, whereas cells on a non-patterned PCL surface were randomly oriented (Figure 2C). Quantitative analysis of average orientation angle (OA) demonstrated significant differences between the non-patterned and patterned groups and significantly higher OA on 50um grooved PCL relative to 25um and 10um grooved films. No significant differences in OA were observed between the 25 and 10um patterned films (Figure 2D). An analysis of the distribution of aligned cells in specific ranges (5° to 15° degree ranges) indicated a higher percentage of cells with the lowest OA (0–5°) on the 10um (86.9%) grooved surface, followed by 25um (79.8%), 50um (32.3%), and control (6.1%) films (Figure 2E). Our results show that cell alignment was highly associated with groove width on 2D PCL films.

2.2 Design of PCL scaffolds with 3D patterned film and 3D printed base

The tooth root is covered with a layer of calcified tissue known as cementum, into which PDL collagen fiber bundles are inserted and further anchored into the alveolar bone. To mimic the known anatomical features of the bone-PDL interphase bordering a tooth root, a scaffold containing compartments for bone and periodontal ligament tissue formation was designed (Figure 3A). In detail, the bone region of the scaffold was adapted for selective laser sintering based on previous parameters established in our laboratory by Park et al.[9] This region was designed to be 5.1×4.1mm with a height of 3.2mm, where the first 2.1mm are part of the base and the remaining 1.1mm on the four corners form an enclosure to contain the film and dentin segment (Figure 3B). Pore sizes were restricted to a minimum of 700um × 700um given the 3D-printer resolution, with composition of the scaffold consisting of PCL mixed with 5% hydroxyapatite (HA) to mimic the mineral-based content of natural bone. The PDL region of the scaffold was designed to provide architectural guidance for cell alignment and subsequent collagen fiber formation using pillars that would act as supportive structures for PDL-like tissue formation between calcified tissues (i.e. bone and dentin). Pillar height was 250um to mimic the average thickness of human PDL tissue. Based on results of cell alignment on 2D-grooved PCL films, pillars were formed with grooves of

60um or 15um and depth of 10 or 30um to investigate effects of groove width and depth on PDL-like tissue formation. A porous salt-leached PCL sponge was included as a negative control, in addition to non-grooved pillars to assess effect of pillars alone on cell and tissue alignment. SEM images indicate the random nature of the porous PCL sponge relative to grooved pillars that present clear boundaries for groove width and depth corresponding to mold design and overall stability of the 250um high features (Figure 3C).

Cementum covers the dentin surface of the tooth root, but this layer was removed from human-derived roots to obtain dentin segments that were cut down to dimensions of the scaffold and positioned over 3D micropatterned film regions (Figure 3D). *In vivo* assessment of tissue alignment within the PDL region was performed using a previously established mouse model utilizing human gingival fibroblast (hGF) cells transduced with adenoviral (Ad) bone morphogenetic protein (BMP)-7 to generate bone formation.[9, 13]

2.3 Mineralized tissue formation in 3-D printed scaffold region *in vivo*

Analysis of bone volume (BV) in samples at 3 and 6 weeks shows a significant difference ($p<0.0001$) in the volume measured encompassing the 3-D printed region of the scaffold versus the volume identified within the entire scaffold region. As evidenced by uCT scans of a scaffold at 6 weeks (Figure 4A) the majority of bone was formed encompassing the scaffold along the 3D-printed PCL walls. However, no significant differences in BV were observed between weeks 3 and 6 for both regions. Tissue mineral density (TMD) indicating maturity of bone showed no differences between regions when comparing both time points, but TMD increased significantly for both the bone region ($p<0.0001$) and entire scaffold ($p<0.001$) from week 3 to week 6 (Figure 4B).

2.4 Histomorphology of soft, mineralized, and cementum-like tissue formation *in vivo*

To delineate the histomorphology of soft and mineralized tissue formation *in vivo*, we performed studies using several staining methods. Hematoxylin and Eosin stains at 3 weeks (data not shown) and 6 weeks indicated soft tissue formation in the region of 3D patterned film, as well as in most of the 3D printed scaffold where bone had not invaded further into the scaffold interior. Trichrome staining of PDL regions revealed randomly-oriented collagenous tissue formation in groups with porous PCL, while pillared PCL films showed fibrous collagen formation with increased directionality towards the dentin segment at 6 weeks (Figure 5A). Staining using DAPI and tubulin-based markers showed high cell density and extracellular matrix formation in the PDL region of the scaffold confined to areas within the inter-pillar distance. Indication of early-stage formation of an immature cementum-like tissue at 6 weeks on the dentin below the PDL region was identified descriptively and also using bone sialoprotein (BSP)-positive staining. The amount of new tissue formation that had cementogenesis-like indicators was minimal overall, with an average length of 337±66um when averaged for all patterned groups, compared to the 2.7mm approximate length of dentin segments.

2.5 Effect of 3D patterned design on cell alignment *in vivo*

Cell alignment *in vivo* was evaluated using nuclear alignment and shape index following immunofluorescence staining of tissue sections. Our data revealed an increasing tendency of

cells along the pillar edge to align perpendicular to the dentin surface with increasing groove depth (Figure 6A), particularly with more cells shown to be aligning further away from the pillar wall. At 3 weeks, all groups had a significantly higher percentage of aligned cells compared to porous PCL, with the same observation present at 6 weeks, except for non-grooved pillars which were not significantly different from the porous sponge. Relative to non-grooved pillars, both of the deeper-grooved groups (60W, 30D and15W, 30D) exhibited significantly higher alignment at 3 weeks ($p<0.001$ and $p<0.01$, respectively). At 6 weeks, the differences in alignment were more apparent, with all grooved pillars irrespective of groove depth (60W, 10D; 15W, 10D; 60W, 30D; and 15W, 30D) showing significantly higher cellular alignment ($p<0.001$ and $p<0.0001$) relative to non-grooved pillars. Likewise, grooved pillars with a depth of 30um also had significantly higher alignment ($p<0.001$) relative to pillars with shallower grooves (Figure 6B).

Nuclear shape index was used to assess nuclear elongation as a complement to the cellular alignment data, with values closer to 1 indicating increased nuclear circularity (Figure 6C)[14]. At 3 weeks, only deeper grooved pillars had significantly higher elongation values compared to both PCL sponge and non-grooved pillars, with the 60W, 30D pillars having more elongated cells relative to non-grooved ($p<0.0001$) and 15W, 30D pillars ($p<0.05$). Only 60W, 30D pillars had significantly higher elongation relative to both of the shallow-grooved pillars at 3 weeks ($p<0.01$). At 6 weeks, all groups had significantly higher elongation relative to cells on the PCL sponge, while all grooved pillars ($p<0.01$–0.0001) also had a significantly lower shape index relative to non-grooved designs. However, no significant differences were noted among the grooved pillar groups, irrespective of groove depth.

Overall, these results demonstrate increased cell alignment further from the pillar boundary in films with grooves compared to non-grooved pillars, with increased alignment in deeper-grooved (30um) pillars compared to shallow-grooved (15um) pillars. This can be attributed to soft tissue maturation and alignment which correspond to a significant increase in overall cell elongation from week 3 to 6, albeit not necessarily perpendicular to the dentin since this quantification considers only cell morphology independent of orientation.

2.6 Effect of 3D patterned design on oriented collagen thickness *in vivo*

The extracellular component of PDL consists of collagen fiber bundles which assist with allowing the tooth to withstand substantial compressive forces. We therefore analyzed collagen thickness oriented along the pillar wall creating a bundle-like structure perpendicular to the dentin segment. Our data showed that collagen thickness at 6 weeks is significantly greater in both deeper-grooved pillar groups with grooves of 60um and 15um compared to non-grooved pillars ($p<0.0001$) (Figure 7). Only one shallow-grooved group (60W, 10D) showed greater thickness relative to 0W, 0D ($p<0.001$). The 60W, 30W group had a total collagen thickness that was significantly higher than other groups, except for its deep-grooved counterpart with narrower grooves of 15um (15W, 30D). These results further reinforce the findings shown with cell alignment at 6 weeks, indicating that groove depth is a more critical parameter than width for encouraging formation of cell alignment and

subsequent increase in oriented collagen fiber density (Figure 1S) at sites of increased cellular orientation.

3. Discussion

Promoting orientation of cells in a specific and structurally-relevant direction via substrate guidance has been shown to stimulate cell behavior and create organized tissues *in vitro* that mimic their native form and function, including cardiac and nerve tissues.[15] Overall, micro- and meso-scale cues have been strongly implicated in aligned cellular and fibrillary collagen formation *in vitro*. Gilchrist et al found that a width of 500um was the maximum *in vitro* meso-scale boundary for guidance of neo-tissue alignment using mesenchymal stem cells.[16] Likewise, highly aligned tissue formation consisting of fibrillary collagen was observed when cells were arranged longitudinally end-to-end. This *in vitro* finding is consistent with our observations *in vivo* of highly aligned cell formation on pillar walls which appears to correspond to increased collagen fiber formation seen with Trichrome staining at sites of increased cell alignment. In fact, our study identified a strong positive correlation (r=0.863, data not shown) between cell alignment and collagen thickness based on values obtained from these measurements (Figure 6–7).

Cellular morphology assessed using both cellular alignment angle and nuclear elongation suggests significant ($p<0.0001$) and overriding effects of groove depth over width. Our results indicate increased preferential alignment of cells *in vivo* on grooved substrates over a non-grooved surface. Nano- and micro-structured groove widths and depths have been extensively investigated using a variety of cells to determine optimum parameters for cell alignment using *in vitro* models.[17] While results can be cell-specific, fibroblasts in particular have been shown to have a nano- and micro-limit of alignment ranging from 50–100nm to 500um.[18] Likewise, several studies have reported increased cell alignment with increasing groove depth, both on nano- and micro-levels.[19] There are strong indications that in particular cases the depth can reinforce, if not override, cellular guidance via groove width. Increase in cell alignment and collagen fiber alignment may also be a factor of the cell's innate ability to align *in vitro* and *in vivo*. Aubin et al showed cells with intrinsic ability to form aligned tissue *in vivo* are more likely to organize into oriented tissue *in vitro* in presence of guidance-based microarchitecture.[20]

Previous studies successful in achieving aligned collagenous tissue formation using substrates with cell-guiding cues have utilized electrospun fibers composed of naturally- and synthetically-derived polymers. Jiang et al reported increased PDL-like tissue formation with mature collagen fibers using aligned PCL-polyethylene glycol (PEG) nanofibers embedded into porous chitosan scaffolds and seeded with bone marrow mesenchymal stem cells.[21] Similar findings have been observed in applications for neural and cardiac tissue regeneration: Koepsell et al noted increased cellular orientation of intervertebral disc-derived cells on increasingly aligned electrospun PCL fibers resulted in higher ECM production, including collagen and glycosaminoglycans,[22] while Ifkovits et al found enhanced collagen alignment on oriented poly(glycerol sebacate) fibers when seeded with cardiocytes and implanted subcutaneously.[23] However, it remains difficult to create three-dimensional scaffolds using these techniques without the presence of a more complex and

customizable system such as a 3-D printer that could position fibers in directions relevant to the anatomical structure of tissue we attempt to model, thereby recapitulating its unique geometric complexity. Additive manufacturing has been used extensively for guided tissue regeneration of PDL-like structures,[10, 12] but micro-level control over scaffold structure is constrained by limited resolution and material selection. To address these limitations, our approach focuses on using a combination of 3-D printing and micropatterning to create a scaffold with the dual function of presenting features on the macro and micro-level for guidance of bulk and oriented tissue formation (i.e. mineralized and soft tissue). To our knowledge, this is the first reported attempt to quantify cell alignment on a micropatterned polymeric construct implanted *in vivo*. While numerous aforementioned publications have signaled the importance and potential of guiding aligned tissue formation using this approach, existing studies have focused on *in vitro* assessment of cellular alignment, without further translation into *in vivo* models.

The development of a 3-D pattern consistent with known geometric parameters of the human periodontal ligament (i.e. 250um average thickness), including presence of collagen I and III fiber bundles that orient perpendicular to the alveolar bone and tooth root (Figure 3), was executed to assess the role of groove width and depth using an *in vivo* model. The 3-D printed bone region and PDL film consisted of defined openings to create porosity within the bulk structure, promoting nutrient exchange and cellular migration between the regions. Seeding of AdBMP-7 expressing hPDL cells in the bone region resulted in bone formation that was mostly external to the interior region of the 3-D printed scaffold as shown using histology and micro-CT analysis (Figures 4 and 5A, respectively), a limitation of the model inherent in the non-localized expression of the growth factor that likely resulted in its diffusion to the exterior regions of the scaffold, as has been observed in other studies.[24, 25] The use of a non-loading model may have contributed to lack of significant increase in bone volume between weeks 3 and 6, although existing bone was found to mature over time, as evidenced by increase in tissue mineral density. Likewise, due to limited bone growth below the PDL region of the scaffold, no integration between the bone and PDL regions was observed. This is an important indicator of bone-ligament complex regeneration and requires future improvements in the design of the bone compartment and localization of bone-stimulating growth factor delivery. Specifically, native bone-PDL integration consists of Sharpey's fiber insertions into osseous tissue that stabilize and connect the soft tissue. A bone region which promotes formation of such attachments below the PDL compartment through incorporation of increased and possibly directional porosity would improve regeneration of this multiphasic tissue complex. To fully and successfully realize periodontal tissue regeneration using a multiphasic scaffold, cementum must be formed along the dentin surface. While our data does not show definitive mature cementum, BSP-positive staining (Figure 5B) does suggest early-stage mineralized, cementum-like tissue formation localized at the boundary between the dentin segment and inter-pillar areas filled with collagenous soft-tissue.

Our results detailing cellular alignment and collagen formation are indicative of the need for guidance of cellular alignment to promote oriented collagen formation *in vivo*. In fact, Wang et al had previously shown that grooved substrates resulted in alignment of synthetized

collagen matrix *in vitro* parallel to the grooves, preceded by the alignment of cells.[26] In this study, we show that this holds true using a micropatterned substrate under *in vivo* conditions, albeit with the added factor of groove depth as an important precursor to the percentage of aligned cells (Figure 6) and resultant thickness of oriented collagenous tissue (Figure 7). It is important to note that while cellular alignment and increased collagen thickness is seen at pillar boundaries, the existing space of 400um between the pillars does not currently allow for aligned tissue formation in that area within a period of 6 weeks. There is likewise the potential of tissue formed between pillars to lose orientation given large inter-pillar distances. Therefore, an improvement to the current patterned film design to better replicate periodontal ligament fiber architecture and increase fiber density would consist of reducing this distance to 100–150um, given that the average thickest formation of oriented collagenous tissue at 6 weeks was ~35um for one side of the 30um-deep grooved pillars. Another area of further study may include an analysis of whether there is a limit to the aligned tissue formation boundary layer away from the pillar surface, since the given results are an indication of the capacity for aligned tissue formation at only 6 weeks *in vivo*.

Future improvements in addition to scaffold morphology would involve introduction of other factors that play a crucial role in formation of functional periodontal ligament, including growth factors such as platelet derived growth factor (PDGF) and mechanical stimulation at physiological levels, which has been show to modulate PDL cell gene activity.[5, 27] Increased control and localization of bone-stimulatory growth factor protein release such as BMP would further benefit osseous tissue formation within the bone compartment. While the use of gene therapy significantly increases sustained growth factor release and stability *in vivo*, further improvements in minimizing growth factor diffusion from the target site would greatly improve its application in scaffold-based therapies.[28] Such strategies could include the direct adsorption or chemical conjugation of BMPs onto the scaffold surface,[29] or tethering of viral vectors expressing BMP genes to PCL surfaces using chemical vapor deposition.[30]

In attempting to transition scaffold-based designs from the bench-top to clinical applications that can benefit patients, use of 3D printing has become a promising strategy for creating customized implants with potential to mimic patient-based bulk defects, even for cases of periodontal therapy.[31] In guided regeneration of ligamentous structures, the combination of 3D printed and micropatterned regions into one construct is an innovative approach that can provide a means of re-establishing the interfacial integrity of aligned tissue formation in bone-ligament complexes. Although the scaffold design used in this study was simplistic relative to a true periodontal defect involving bone resorption, it can be easily adapted to more complex defects using patient-based computed tomography scans to design the 3D printed region, and create an overlay of a micropatterned film in the region of missing PDL. The results of our study indicating the importance of groove depth over width for aligned tissue formation *in vivo* can play a vital role in the establishment of a design that can incorporate this cell-guiding parameter into future grafts meant for the purpose of inducing structurally-relevant alignment of PDL tissue. Future translation of micropatterned constructs into the clinic may provide greater opportunities for more controlled tissue regeneration using not only ridge-groove structures, but also other relevant designs that can

help orient tissue based on incorporated material boundaries. The combination of a custom-designed 3-D printed scaffold and a micropatterned region fit to control the structural integrity of new tissue growth is a clinically-relevant approach that holds significant potential for regeneration of collagenous tissue not only in periodontal and orthopaedic applications, but other areas of tissue engineering with a strong focus on improving collagen fiber orientation as it relates to tissue structure and function.

4. Conclusion

In summary, the findings from this preclinical study indicate that groove micro-depth has a significant effect on guiding cellular alignment and collagenous tissue orientation *in vivo*, overriding the effects of groove micro-width. The 3-D patterned scaffold conceived and designed in this study further presents a novel and unique combination of 3-D printing and micropatterning to enhance the micro- and macro-level design of scaffolds with the aim of regenerating multiple tissues and their interfaces. Using a combination of gene therapy and topographical guidance cues to achieve osseous tissue formation and oriented collagen fibers has potential for bone-ligament regeneration for treatment of periodontal osseous defects. Overall, these findings are supportive of the advantageous effects of using 3-D printed, micropatterned substrates as architectural templates for guided regeneration of oriented collagenous tissues. This approach may have significant potential for clinical applications in the development of bone-ligament constructs for dental and orthopaedic clinical scenarios.

5. Experimental Section

5.1 Preparation and imaging of patterned 2D and 3D films

Polycaprolactone films (2D) were prepared by dissolving PCL (MW: 43–50 kDA) in chloroform (Sigma) (10% w/v) and spin coating the solution (1st coat at 100 rpm for 8 sec, 2nd coat at 800 rpm for 20 sec) onto polydimethylsiloxane (PDMS) (Sylgard 184; Dow Corning) designed via established soft lithography techniques with grooves ranging from 10–50um in width, 10 um in depth.[32] Briefly, a CAD-based program (LEdit) was used to design micropatterns and define the silicon and SU-8 master molds with standard photolithography. All steps for mold fabrication were performed at Lurie Nanofabrication Facility (University of Michigan, Ann Arbor, MI). To transfer the pattern of SU-8 molds onto a flexible polymer, PDMS was mixed in a ratio of 10:1 v/v of base to curing agent, degassed under vacuum, poured onto molds, and cured (65°C). PDMS was then peeled from SU-8 mold and used as a mold to pattern PCL. Control films were made by spin coating PCL onto non-patterned PDMS stamps. Similarly, 3D micropatterned PCL films were prepared by casting PCL solution onto PDMS molds with grouped arrays of five different designs: (1) 400×400μm non-grooved square pillars 250um in height spaced 400um apart, (2) same pillars with 10um deep, 60um wide grooves on the perimeter, (3) pillars with 10um deep, 15um wide grooves, (4) pillars with 30um deep, 60um wide grooves, and (5) pillars with 30um deep, 15um wide grooves. SEM was performed at the Microscopy and Image Analysis Laboratory (University of Michigan) using an Amray FE 1900 SEM to image patterned 3D films which were gold sputter coated and observed at an acceleration voltage of 5kV.

5.2 Surface treatment and MTS assay

Amination of films was performed using 10% (w/v) 1,6-hexanediamine for 1hr at 37°C. Hydrolysis was achieved using 1M sodium hydroxide solution (4 hours at room temperature). Fibronectin treatment consisted of incubating films overnight in phosphate buffered saline (1X PBS), exposed to bovine-derived fibronectin solution (10ug/mL, Sigma) for 30min at 37°C, with washes in PBS. All non-patterned films were sterilized in 70% ethanol for 30 min and washed in sterile dH_20 prior to treatment, and again washed in sterile dH_2O post-treatment with amination or hydrolysis. Prior to cell seeding, all films were incubated for 30 min in cell culture media consisting of Dulbecco's Modified Eagle Medium with glutamine (DMEM), 10% fetal bovine serum (FBS), and antibiotics (100 units/ml penicillin and 100 mg/ml streptomycin). Human PDL cells (passages 4–6) were seeded at a density of 1.5×10^4 cells/film on non-treated and surface-treated PCL films (n=3). Cell adhesion and proliferation was assessed at days 1 and 5 post-seeding by adding MTS solution (CellTiter 96® Aqueous One Solution, Promega Corp, Madison, WI) to films washed three times in PBS, and reading triplicates at 490 nm after 2 hr incubation (37°C).

5.3 In vitro cell culture and alignment analysis on 2D patterned films

To assess PDL cell alignment on patterned 2D substrates, films were seeded with hPDL cells (passages 4–6, 1.2×10^4 cells/film) stained with DilC(12)3 (10ug/mL, BD Biosciences, Bedford, MA, USA). Prior to cell seeding, films were surface treated with hydrolysis and fibronectin as described previously. At 24hrs post-seeding, films were washed three times in PBS and imaged using fluorescence microscopy (Nikon Eclipse 50i, Nikon Instruments Inc). ImageJ (NIH) was used to evaluate cell orientation angle (OA) between 0° and 90° via a virtual axis placed in each cell, with the angle between the axis of the cell and direction of the pattern (corresponding to 0°) measured for all films (n=4). Results from OA analysis were used to inform the design of 3D pillared PCL films.

5.4 Preparation of biphasic integrated scaffold with 3D-printed and 3D patterned PCL regions

To model the interphase between alveolar bone and periodontal ligament, a biphasic scaffold based on a previous design[9] was fabricated with individual compartments for bone and PDL growth using 3-D printed PCL structures for a bone compartment combined the aforementioned 3D micropatterned films for a PDL interface, respectively. PCL scaffold geometry for 3-D printing was designed using CAD-based software (NX 7.5, Siemens PLM Software), with base dimensions of 5.1×4.1×2.1 mm, a 1.1 mm high enclosure to contain the PCL film, and pore openings of 0.7×0.7mm. Selective laser sintering (SLS) was used to fabricate the bone compartment using PCL powder (43–50kDa; Polysciences, Warrington, PA) and 4 wt% hydroxyapatite (Plasma Biotal Limited).[25, 33] To assemble the biphasic scaffold, a micropatterned 3D PCL film (3.6×2.8 mm) containing an array of 20 square pillars and 400um circular pores was directly fitted onto the 3D printed PCL bone region. The four corners of the upper bone scaffold region (Figure 3B) anchor, stabilize, and integrate the PCL film in place.

5.5 *In vivo* implantation and specimens harvest

One day prior to implantation, PCL films was treated with fibronectin and seeded with hPDL cells as previously described using *in vitro* cell culture to allow for cell attachment and alignment. The day of surgery, two surgical pockets were made on the dorsa of immunodeficient 6 week-old NIH III nude mice (20–25g; Charles River Laboratories, Wilmington MA) for subcutaneous scaffold implantation (n=6 per time point) under isofluorane anesthesia. The bone region was seeded with Ad-BMP7 (MOI=500) expressing hGFs (2.5×10^5cells in 8uL fibrinogen mixed with 2ul thrombin) and the PDL region seeded with hPDLs (1.5×10^5cells in 15mL fibrinogen mixed with 3uL thrombin). A human-derived dentin segment surface-treated with 37% orthophosphoric acid and trimmed to scaffold size was press-fit onto 3D patterned PCL film to ensure contact between pillars and dentin surface. Dentin segments derived from healthy human teeth were obtained in accordance with a University of Michigan-Institutional Review Board (IRB) approved protocol, and animal studies were performed with approval from University of Michigan-University Committee on Use and Care of Animals (UM-UCUCA) according to ARRIVE guidelines for preclinical studies. Samples were harvested at 3 and 6 weeks and fixed in 10% buffered formalin phosphate solution for 2 days before being transferred into 70% ethanol.

5.6 Micro-computed tomography (Micro-CT), histomorphometry, immunofluorescence, and immunohistochemistry

Tissue-fixed specimens were embedded in alginate, scanned using micro-CT (Scanco Medical) at a resolution of 12um, at 70kV energy and 114uA intensity, and calibrated to Hounsfield units (HU). Bone volume (BV) and tissue mineral density (TMD) were determined for internal and external regions of the bone compartment using Microview software (Parallax Innovations) with a threshold of HU=1050 for bone. After scanning, samples were decalcified in 10% EDTA, embedded in paraffin, and cut into 5um sections for histological analysis using hematoxylin and eosin (H&E) and Masson's trichrome staining to evaluate fibrous tissue orientation and collagen formation, respectively. Immunofluorescence staining was performed using 4',6-diamidino-2-phenylindole (Prolong Gold Antifade Reagent with DAPI; Life Technologies) to label cell nuclei and anti-tubulin antibody with AlexaFluor488 (1:100 dilution, Abcam Inc, Cambridge MA) to label microtubules. Stained slides were imaged using fluorescence microscopy (Nikon Eclipse 50i) to capture cell nuclear alignment for all groups using a specified ROI (150um×250um). ImageJ was used to quantify percentage of cells aligned perpendicular to the dentin segment, with cells considered aligned at an angle of ±20° from the perpendicular at 90° (i.e. $70° \leq \times \leq 110°$, where×is the alignment angle). Nuclear shape index was used to assess cell nuclear elongation. ImageJ was used to threshold the images and run an analysis of elongation based on a measure of circularity ($C=4*\pi*\text{area}/\text{perimeter}^2$, where C=1 indicates a circle)[14]. Masson's trichrome images were further used to assess thickness of collagen bundles oriented perpendicular to dentin segment at sites bordering the grooved and non-grooved pillars for samples obtained at 6 weeks.

Formation of cementum-like tissue was quantified using H&E sections and further assessed via immunohistochemical analysis of bone sialoprotein (BSP) positive staining using deparaffinized sections. Before immunostaining, rehydrated sections were treated with 3%

hydrogen peroxide and blocked in bovine serum albumin to reduce non-specific binding. Sections were exposed to primary antibody (1:200, Anti-bone sialoprotein antibody, Abcam, Cambridge, MA) for 24 hours at 4°C, washed in PBS with 0.2% Triton-X, and exposed to secondary antibody for 1hr (Goat Anti-rabbit IgG H&L (HRP), Abcam). After washes in PBS with Triton-X, sections were briefly exposed to a chromogen/substrate solution (DAB substrate kit, Abcam) and counter-stained (Hematoxylin, Sigma-Aldrich).

5.7 Statistical analysis

Data were expressed as mean ± standard deviation of the mean. One-way analysis of variance (ANOVA) with post hoc Tukey's multiple comparison method was used to perform comparative analysis, with a p-value <0.05 ($\alpha<0.05$) considered significant.

Supplementary Material

Refer to Web version on PubMed Central for supplementary material.

Acknowledgments

This study was supported by the National Institute of Health/National Institute for Dental and Craniofacial Research (NIH/NIDCR DE 13397). SPP acknowledges support from the National Science Foundation (NSF GRFP 1256260). The authors would like to thank James Sugai (Department of Periodontics and Oral Medicine, University of Michigan School of Dentistry), Shabnam Behdin, and Erin Heffez for assistance with *in vitro* and *in vivo* experiments.

References

1. a) Bettinger CJ, Langer R, Borenstein JT. Angew. Chem. Int. Ed. Engl. 2009; 48:5406. [PubMed: 19492373] b) Hui EE, Bhatia SN. Proc. Natl. Acad. Sci. USA. 2007; 104:5722. [PubMed: 17389399] c) Hoehme S, Brulport M, Bauer A, Bedawy E, Schormann W, Hermes M, Puppe V, Gebhardt R, Zellmer S, Schwarz M, Bockamp E, Timmel T, Hengstler JG, Drasdo D. Proc. Natl. Acad. Sci. USA. 2010; 107:10371. [PubMed: 20484673]
2. Eke PI, Dye BA, Wei L, Thornton-Evans GO, Genco RJ. J. Dent. Res. 2012; 91:914. [PubMed: 22935673]
3. a) Kaigler D, Cirelli JA, Giannobile WV. Expert Opin. Drug. Deliv. 2006; 3:647. [PubMed: 16948560] b) Rios HF, Lin Z, Oh B, Park CH, Giannobile WV. J. Periodontol. 2011; 82:1223. [PubMed: 21284553]
4. Hamilton DW, Oates CJ, Hasanzadeh A, Mittler S. PLoS One. 2010; 5:e15129. [PubMed: 21152020]
5. Yu N, Prodanov L, te Riet J, Yang F, Walboomers XF, Jansen JA. J. Periodontol. 2013; 84:1504. [PubMed: 23215671]
6. Ivanovski S, Vaquette C, Gronthos S, Hutmacher DW, Bartold PM. J. Dent. Res. 2014; 93:1212. [PubMed: 25139362]
7. a) Hacking S, Khademhosseini A. J. Dent. Res. 2009; 88:409. [PubMed: 19493883] b) Stevens MM, George JH. Science. 2005; 310:1135. [PubMed: 16293749]
8. Wegst UG, Bai H, Saiz E, Tomsia AP, Ritchie RO. Nat. Mater. 2015; 14:23. [PubMed: 25344782]
9. Park CH, Rios HF, Jin Q, Bland ME, Flanagan CL, Hollister SJ, Giannobile WV. Biomaterials. 2010; 31:5945. [PubMed: 20471083]
10. Park CH, Rios HF, Jin Q, Sugai JV, Padial-Molina M, Taut AD, Flanagan CL, Hollister SJ, Giannobile WV. Biomaterials. 2012; 33:137. [PubMed: 21993234]
11. a) Costa PF, Vaquette C, Zhang Q, Reis RL, Ivanovski S, Hutmacher DW. J. Clin. Periodontol. 2014; 41:283. [PubMed: 24304192] b) Vaquette C, Fan W, Xiao Y, Hamlet S, Hutmacher DW, Ivanovski S. Biomaterials. 2012; 33:5560. [PubMed: 22575832]

12. Lee CH, Hajibandeh J, Suzuki T, Fan A, Shang P, Mao JJ. Tissue Eng Part A. 2014; 20:1342. [PubMed: 24295512]
13. Jin QM, Anusaksathien O, Webb SA, Rutherford RB, Giannobile WV. J. Periodontol. 2003; 74:202. [PubMed: 12666709]
14. Versaevel M, Grevesse MT, Gabriele S. Nat. Commun. 2012; 3:671. [PubMed: 22334074]
15. Nikkhah M, Edalat E, Manoucheri S, Khademhosseini A. Biomaterials. 2012; 33:5230. [PubMed: 22521491]
16. Gilchrist CL, Ruch DS, Little D, Guilak F. Biomaterials. 2014; 35:10015. [PubMed: 25263687]
17. Flemming RG, Murphy CJ, Abrams GA, Goodman SL, Nealey PF. Biomaterials. 1999; 20:573. [PubMed: 10213360]
18. a) Biela SA, Su Y, Spatz JP, Kemkemer R. Acta. Biomater. 2009; 5:2460. [PubMed: 19410529] b) Leclerc A, Tremblay D, Hadjiantoniou S, Bukoreshtliev NV, Rogowski JL, Godin M, Pelling AE. Biomaterials. 2013; 34:8097. [PubMed: 23899447] c) Loesberg WA, te Riet J, van Delft FC, Schon P, Figdor CG, Speller S, van Loon JJ, Walboomers XF, Jansen JA. Biomaterials. 2007; 28:3944. [PubMed: 17576010]
19. a) Clark P, Connolly P, Curtis AS, Dow JA, Wilkinson CD. J. Cell Sci. 1991; 99(Pt 1):73. [PubMed: 1757503] b) Fraser SA, Ting YH, Mallon KS, Wendt AE, Murphy CJ, Nealey PF. J. Biomed. Mater. Res. A. 2008; 86:725. [PubMed: 18041718] c) Teixeira AI, Abrams GA, Bertics PJ, Murphy CJ, Nealey PF. J. Cell Sci. 2003; 116:1881. [PubMed: 12692189]
20. Aubin H, Nichol JW, Hutson CB, Bae H, Sieminski AL, Cropek DM, Akhyari P, Khademhosseini A. Biomaterials. 2010; 31:6941. [PubMed: 20638973]
21. Jiang W, Li L, Zhang D, Huang S, Jing Z, Wu Y, Zhao Z, Zhao L, Zhou S. Acta Biomater. 2015; 25:240. [PubMed: 26188325]
22. Koepsell L, Remund T, Bao J, Neufeld D, Fong H, Deng Y. J. Biomed. Mater. Res. A. 2011; 99:564. [PubMed: 21936046]
23. Ifkovits JL, Wu K, Mauck RL, Burdick JA. PLoS One. 2010; 5:e15717. [PubMed: 21203510]
24. Saito E, Suarez-Gonzalez D, Murphy WL, Hollister SJ. Adv. Healthc. Mater. 2015; 4:621. [PubMed: 25515846]
25. Williams JM, Adewunmi A, Schek RM, Flanagan CL, Krebsbach PH, Feinberg SE, Hollister SJ, Das S. Biomaterials. 2005; 26:4817. [PubMed: 15763261]
26. Wang JH, Jia F, Gilbert TW, Woo SL. J. Biomech. 2003; 36:97. [PubMed: 12485643]
27. Kim SG, Kim SG, Viechnicki B, Kim S, Nah HD. J. Clin. Periodontol. 2011; 38:1130. [PubMed: 22092876]
28. Pilipchuk SP, Plonka AB, Monje A, Taut AD, Lanis A, Kang B, Giannobile WV. Dent. Mater. 2015; 31:317. [PubMed: 25701146]
29. a) Patel JJ, Flanagan CL, Hollister SJ. Tissue Eng. Part C Methods. 2015; 21:489. [PubMed: 25345571] b) Patel JJ, Modes JE, Flanagan CL, Krebsbach PH, Edwards SP, Hollister SJ. Tissue Eng. Part C Methods. 2015; 21:889. [PubMed: 25809081] c) Zhang H, Migneco F, Lin CY, Hollister SJ. Tissue Eng. Part A. 2010; 16:3441. [PubMed: 20560772]
30. Hu W-W, Elkasabi Y, Chen H-Y, Zhang Y, Lahann J, Hollister SJ, Krebsbach PH. Biomaterials. 2009; 30:5785. [PubMed: 19596152]
31. a) Park CH, Rios HF, Taut AD, Padial-Molina M, Flanagan CL, Pilipchuk SP, Hollister SJ, Giannobile WV. Tissue Eng. Part C Methods. 2014; 20:533. [PubMed: 24188695] b) Rasperini G, Pilipchuk SP, Flanagan CL, Park CH, Pagni G, Hollister SJ, Giannobile WV. J. Dent. Res. 2015; 94(9 Suppl):153S. [PubMed: 26124215]
32. Qin D, Xia Y, Whitesides GM. Nat. Protoc. 2010; 5:491. [PubMed: 20203666]
33. a) Partee B, Hollister SJ, Das S. Journal of Manufacturing Science and Engineering. 2006; 128:531.b) Zopf DA, Hollister SJ, Nelson ME, Ohye RG, Green GE. N. Engl. J. Med. 2013; 368:2043. [PubMed: 23697530]

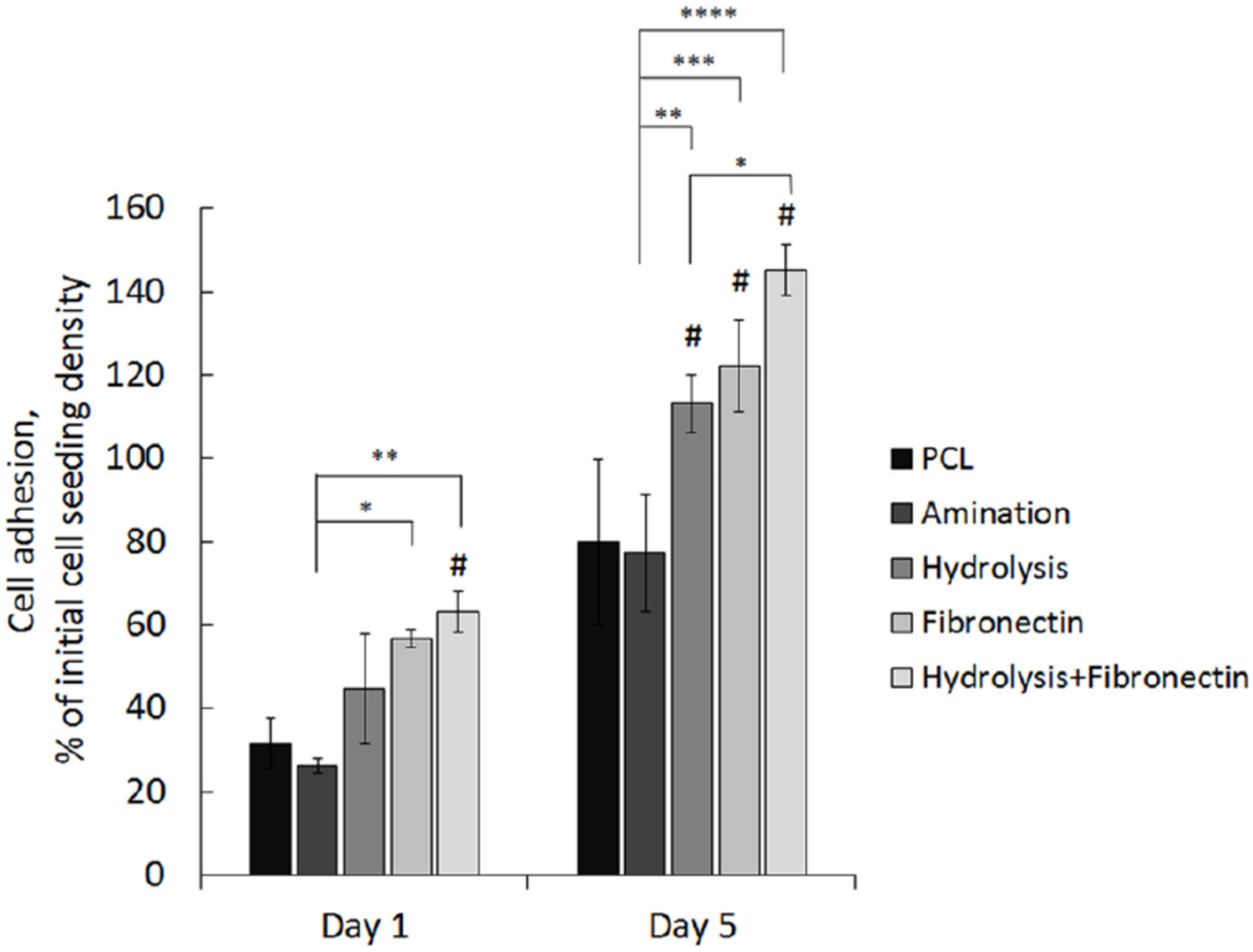

Figure 1.

Surface treatment of PCL films using aminolysis, hydrolysis, fibronectin coating, and combined treatment of hydrolysis and fibronectin assessed to determine conditions for increased hPDL cell attachment. Data shows mean percentage of ligament progenitor cells adhered to non-treated PCL films *in vitro* versus surface-treated PCL at 1 and 5 days post-seeding. (Error bars: ± SD; ** $p<0.01$; *** $p<0.001$, **** $p<0.0001$; # indicates $p<0.05$ relative to non-treated PCL film at each timepoint; n=3).

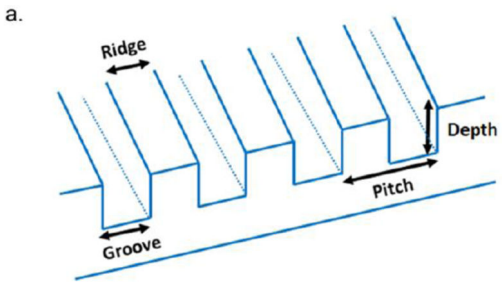

Mold #	Growth width	Groove depth	Pitch
1	10 um	10 um	20 um
2	25 um	10 um	50 um
3	50 um	10 um	100 um

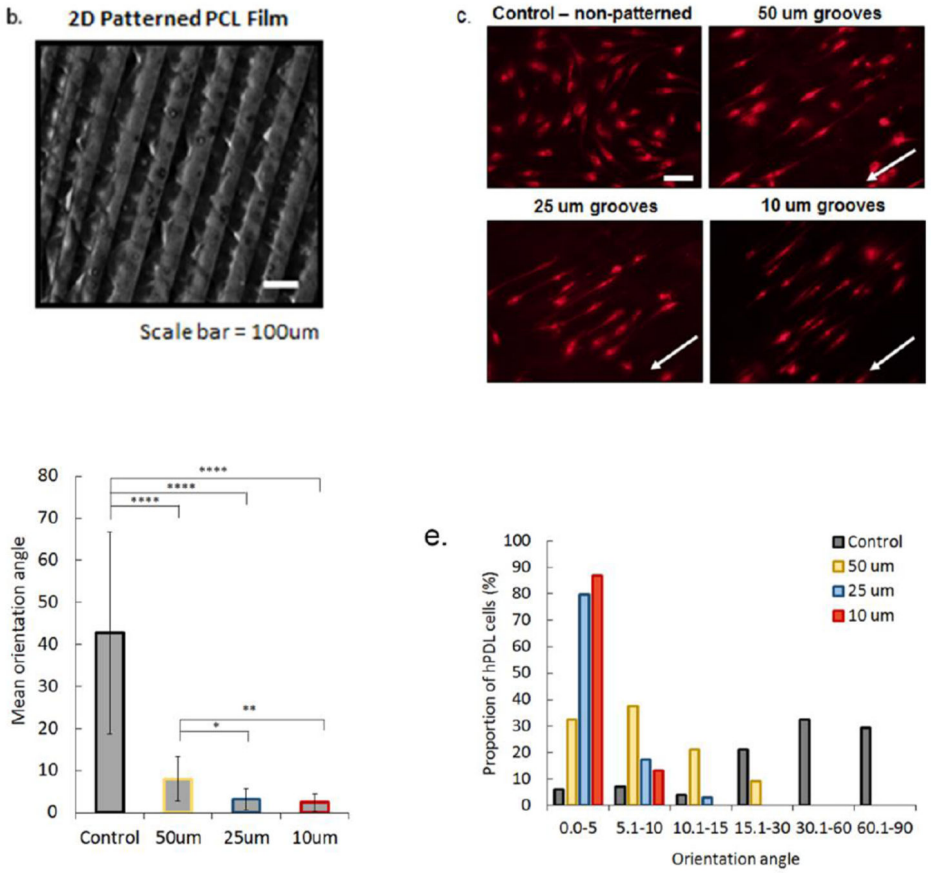

Figure 2.

Micropatterned 2D PCL film design was used to determine effects of groove width on hPDL cell alignment *in vitro*. Films were patterned using three different molds (**a**) to embed grooved features onto the polymer surface (**b**, surface with 50um wide grooves, Nikon SMZ18 stereo microscope). DilC(12)-3 stained hPDL cells seeded on hydrolyzed and fibronectin treated PCL films with non-grooved (control) and grooved surfaces (**c**). White arrows indicate direction of grooves (scale bar=50um). Average orientation of hPDL cells on control (non-patterned), 50 um, 25 um, and 10 um grooved PCL films, where 0° indicates

complete alignment with pattern and 90° indicates a cell that is perpendicular to a groove (**d**). Proportion of hPDL cells within a specific orientation angle for all PCL film groups, with 0–5° groups indicating highest alignment of cells within grooved microfeatures (**e**). (Error bars: ± SD; * $p<0.05$; ** $p<0.01$; **** $p<0.0001$).

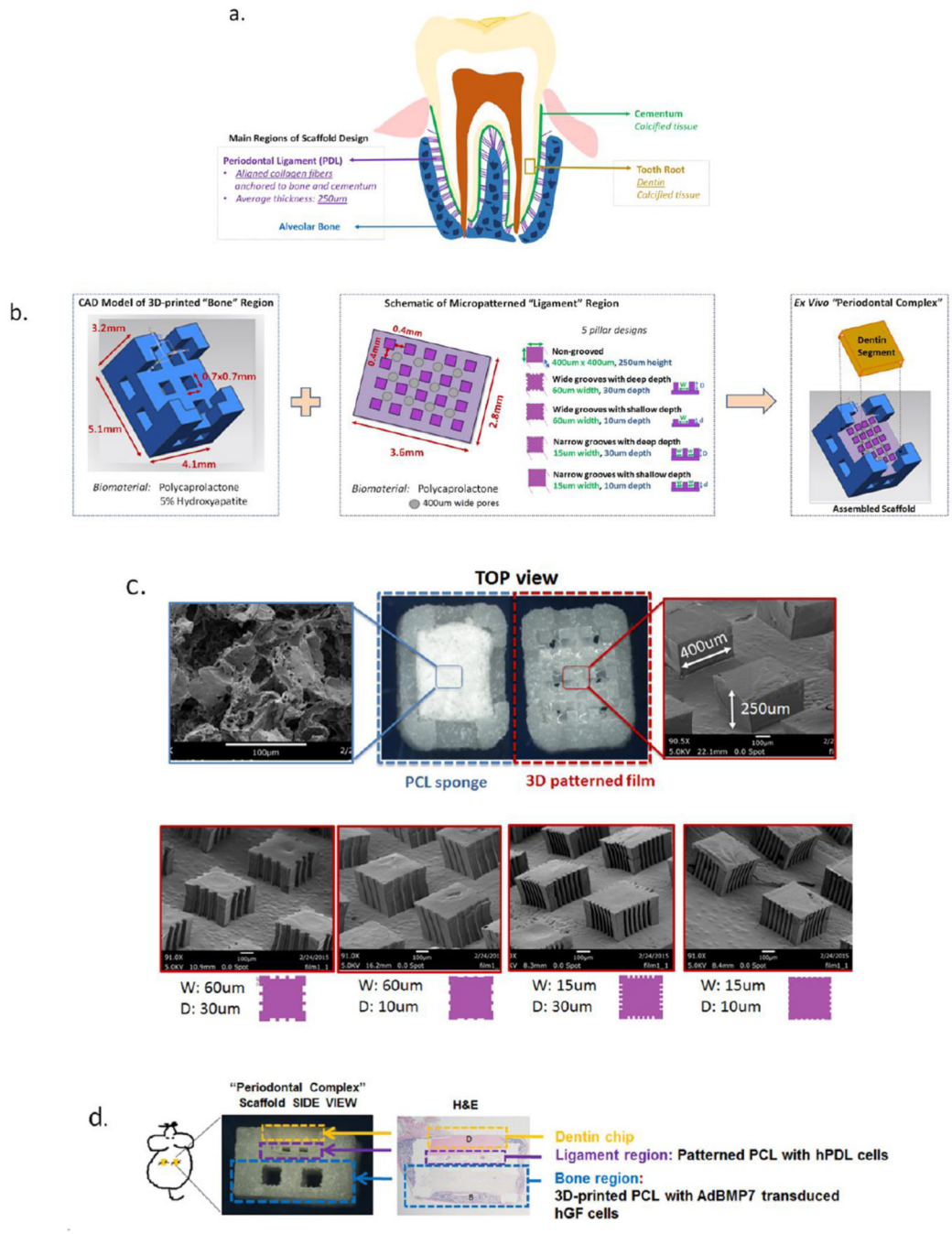

Figure 3.

Schematic design of the scaffold intergrating 3D printed and micropatterned regions for the bone-ligament oral complex. Anatomical features of the alveolar bone-periodontal ligament interphase present innately at the tooth root surface **(a)** were used to design a scaffold combining a 3D printed PCL region and a 3D patterned PCL film for the bone and PDL regions, respectively **(b)**. A total of six groups **(c)** were tested *in vivo* by varying the geometry (width, W and depth, D of the grooves) of the PCL in the PDL region of the scaffold: (1) random-porous, salt-leached PCL sponge, (2) 400×400 um square pillars

250um in height, (3) square pillars with 60um wide and 30um deep grooves, (4) pillars with 60um wide and 10um deep grooves, (5) pillars with 15um wide, 30um deep and 15um wide, 10um deep (6) grooves. **(d)** An ex vivo mouse model was used to subcutaneously implant the combined scaffold to promote bone (B) and periodontal ligament formation, with a dentin chip (D) press-fit on top of the combined scaffold after cell-seeding the PDL region prior to implantation.

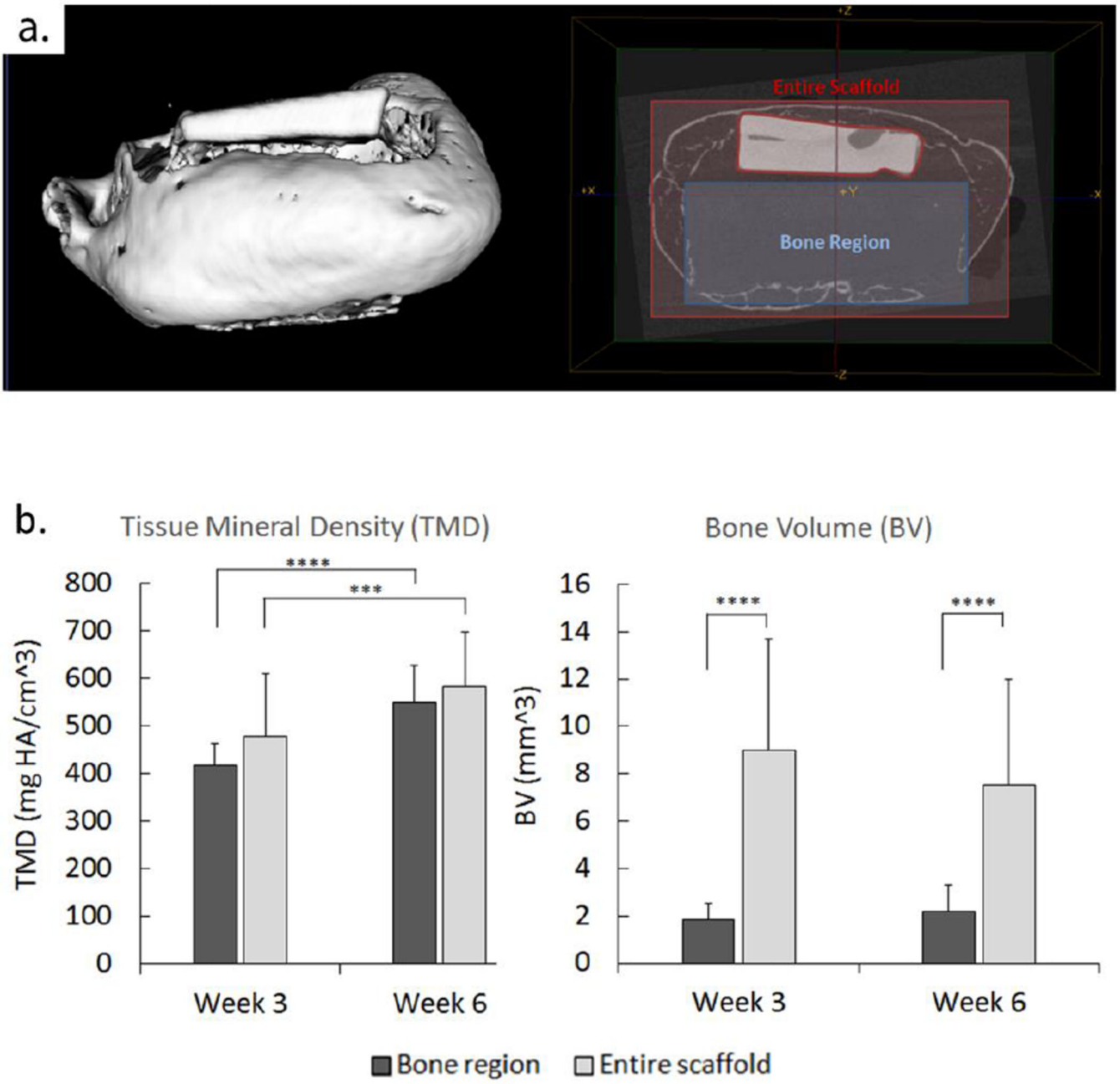

Figure 4.

Formation of bone in the 3D printed scaffold region seeded with adenoviral BMP7 transduced gingival fibroblasts. Micro-computed tomography (uCT) of implanted scaffolds was used for bone volume (BV) and tissue mineral density (TMD) analysis of osseous tissue growth in vivo in the bone region of the scaffold **(a)** compared to the formation of tissue in the entire scaffold external to bone region at 3 and 6 weeks post-harvesting **(b)**. (Error bars: ± SD; *** $p<0.001$, **** $p<0.0001$; n=5–6).

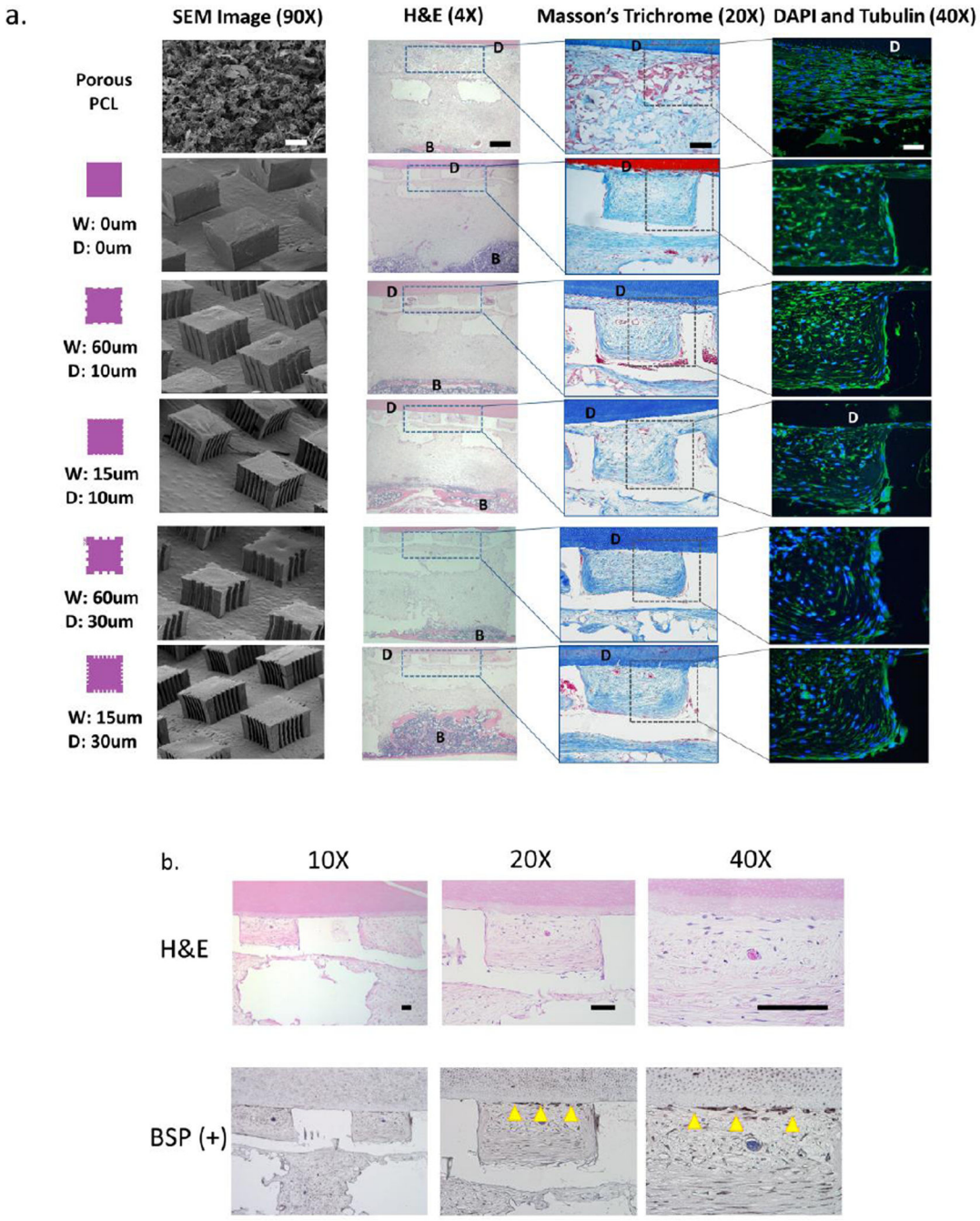

Figure 5.

Histomorphological assessment of soft and mineralized tissue formation in the micropatterned PDL and 3D printed bone scaffold compartments, respectively. **(a)** H&E, Masson's trichrome, and DAPI (blue)/tubulin(green) staining was performed to assess bone (B) and tissue formation, collagen alignment, and cellular alignment in the region of the PCL film or sponge at 3 and 6 weeks (images shown are at 6 week timepoint only). Note the formation of fibers approaching the dentin surface and bone more distant in the bone region of the scaffold (near bottom of the H&E sections). **(b)** Formation of cementum-like tissue

newly-deposited at the dentin (D) surface was observed on week 6 samples using H&E staining and immunohistochemical analysis for bone sialoprotein (BSP) positive expression. Scale bar = 100um.

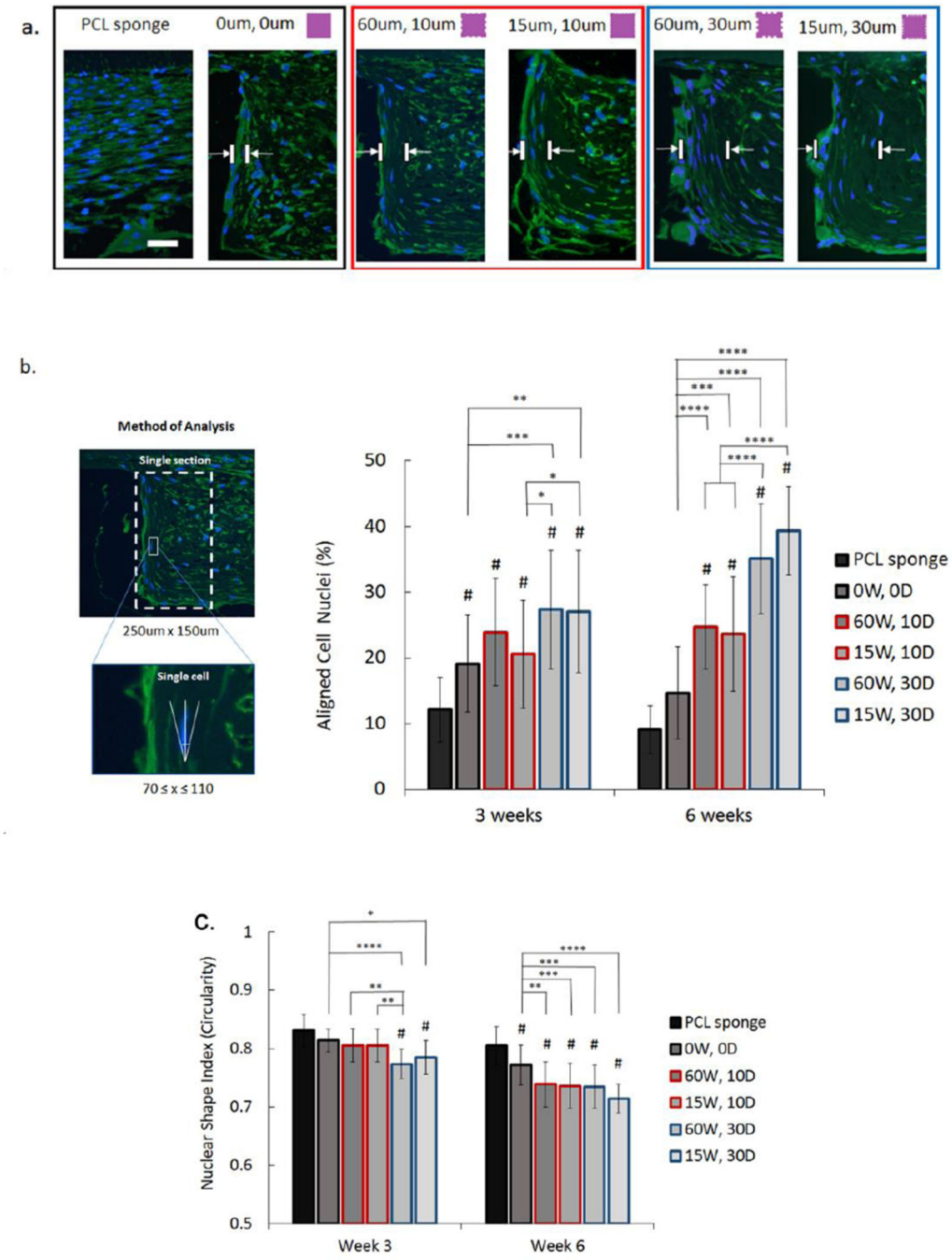

Figure 6.

Cell alignment and nuclear shape index assessed using immnufluorescence staining at 6 weeks. **(a)** DAPI (blue) and tubulin (green) shows increased cell alignment further from the pillar boundary in films with grooves compared to non-grooved pillars, and in films with deep grooves (30um) compared to more shallow grooves (10um). Scale bar = 50um. **(b)** Mean percentage of aligned cell nuclei (within 20° of preferred perpendicular orientation: 70°≤x≤110°) in vivo on PCL sponge, non-grooved pillars (0W, 0D), and grooved pillars (60 um and 15um wide (W) grooves) with varying groove depths (D) (10 um—red outline, and

30um—blue outline). **(c)** Mean nuclear shape index analysis indicating cellular elongation in vivo on all groups based on measure of nuclear circularity ($C=4*\pi*area/perimeter^2$). (Error bars: ± SD; ** $p<0.01$; *** $p<0.001$, **** $p<0.0001$; # indicates $p<0.05$ relative to PCL sponge at each timepoint; n=5 in each group).

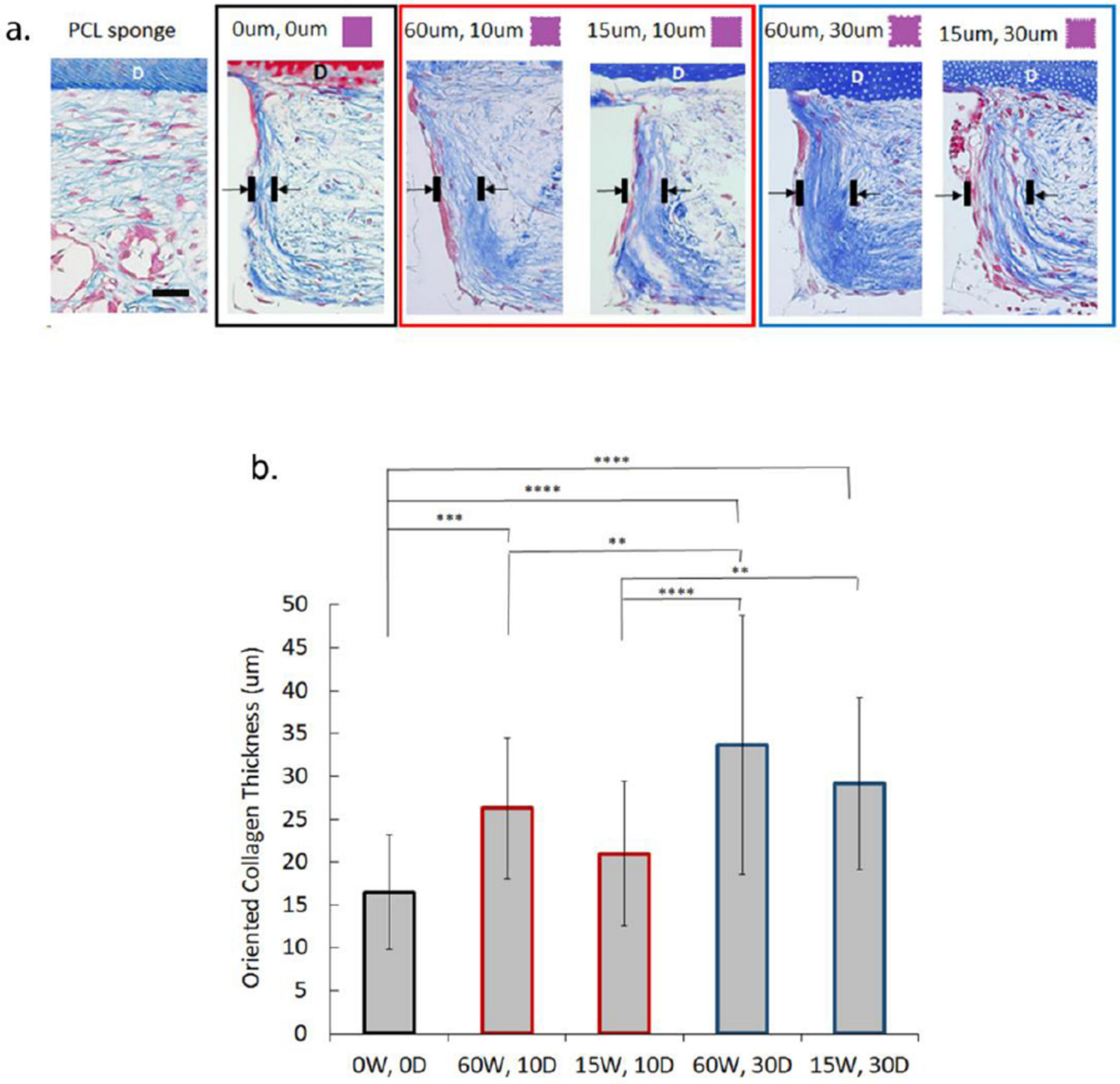

Figure 7.

Collagen thickness at inter-pillar distances bordering grooved or non-grooved features used to determine oriented tissue formation at 6 weeks *in vivo*. **(a)** Masson's Trichrome stining of samples indicates increased collagen orientation perpendicular to dentin (D) chip at the pillar boundary in the presence of grooves (scale bar = 100um). **(b)** Mean thickness (um) of oriented collagen bundles in vivo at non-grooved (0W, 0D) and grooved (15–60um wide, 10–30um deep) pillar borders at 6 weeks based on Masson's Trichrome staining. (Error bars: ± SD; ** $p<0.01$; *** $p<0.001$, **** $p<0.0001$; n=5).